



Research Article

Processing and characterization of polypropylene (PP)/ethylene–vinyl acetate (EVA) blend-based glassy carbon (GC) composites

Erick Gabriel Ribeiro dos Anjos¹ · Guilherme Ferreira de Melo Morgado¹ · Leonardo de Souza Vieira¹ · Gabriel Portilho Monteiro de Souza¹ · Maria Fernanda Romeu Lino de Souza¹ · Iury Araújo Nogueira¹ · Lina Dayse Alcantara Rodrigues¹ · Yves Nicolau Wearn¹ · Fabio Roberto Passador¹

Received: 9 March 2020 / Accepted: 8 July 2020 / Published online: 16 July 2020
© Springer Nature Switzerland AG 2020

Abstract

Polypropylene (PP)/ethylene–vinyl acetate (EVA) (60/40) blends-based glassy carbon (GC) composites with different contents of GC (0.1 to 5 wt%) were melting processed in a twin-screw extruder and the thermal, mechanical, electrical and morphological properties were evaluated to verify the effectiveness of the addition of GC as filler. Moreover, the effect of the addition of maleic anhydride grafted polypropylene (PP-*g*-MA) as a compatibilizer agent was also verified. The composites presented dispersed phase morphology with preferential localization of GC on interfacial regions and into the EVA phase. The mechanical properties were improved with the addition of PP-*g*-MA as a compatibilizer agent for the blend and the addition of GC had little influence on these properties. The results obtained from thermal properties revealed that the GC contributes to the increase in the degree of crystallinity and thermal stability of the composites. The addition of 0.1 wt% of GC increased the elastic modulus and the ultimate tensile strength without loss in the impact strength when compared to the compatibilized blend. The addition of GC increases a decade of magnitude in the electrical conductivity of the PP/EVA blends.

Keywords Glassy carbon · Filler · Polypropylene · Ethylene–vinyl acetate · Polymer blend · Composites

1 Introduction

Glassy carbon (GC) is a non-graphitizable carbonaceous material constituted microscopically by the stacking of sp^2 -hybridized carbon hexagonal structures [1]. These arrangements form layers that are twisted and tangled resulting in the so-called turbostratic structure, which is responsible for giving the material good chemical, mechanical and electrical properties such as corrosion resistance, hardness, and high electrical conductivity [1, 2]. Nowadays, GC is a promising material in the development of several applications: hydrocephalic and heart valves, surface mirrors in optical systems, camera lenses, high-temperature

furnace elements, laboratory crucibles, and solid-state batteries (electrode material) [3–5].

The production of GC is based on the carbonization of cellulose or different thermosetting resins, such as phenolic and poly(furfuryl alcohol) resins, at temperatures up to 1000 °C [6, 7]. Micro- and mesoporous GC, known as monolithic GC, can be produced even in complex shapes. However, a rigid control of the processing parameters is required, since the generation of resin decomposition products and high heating rates lead, respectively, to the formation of macropores and the appearance of tensions and discontinuities within the material [7].

Carbonaceous materials such as carbon black [8–10], carbon nanotubes [11] and graphene [12] are being

✉ Fabio Roberto Passador, fabio.passador@unifesp.br | ¹Polymer and Biopolymer Technology Laboratory (TecPBio), Universidade Federal de São Paulo (UNIFESP), Talim, 330, São José dos Campos, SP 12231-280, Brazil.



extensively studied as a conductive filler to improve polymers performance in composites [13], increasing electrical conductivity and the mechanical properties for packaging applications, mainly antistatic packaging [14]. In this way, GC can also be applied as a conductive filler; however, its application in polymer matrices is relatively recent and has few studies regarding this application in the literature [15, 16]. Szeluga et al. [15] obtained composites employing different GC contents (2.5 and 5.0 wt%) in a thermosetting matrix of epoxy resin and observed an improvement in elastic modulus and electrical conductivity in the composites. The materials were obtained using an ultrasonic treatment, three roll mills, and high shear homogenizer.

Santos et al. [16] used the GC as conductive and antistatic filler to reduce the electrical resistivity of low-density polyethylene (LDPE). The LDPE/GC composites were prepared with different GC contents (0, 0.5, 1, 5, 10, 15, and 20 wt%) in a high-speed mixer. It was verified that the GC particles were homogeneously dispersed and distributed in the polymer matrix, therefore allowing the achievement of a relatively low percolation threshold (0.5 wt% of GC) and electrical resistivity of 2 orders of magnitude lower than the neat LDPE, which qualifies the material to be used as an antistatic package.

Polymer blending is another strategy to modify and improve polymers, which is cost-effective and largely applicable in the industry [17, 18]. Polymer blends allow joining the best properties of two or more different polymers (or copolymers) in a new material, bypassing some disadvantages of applying the neat material, for example, low impact strength, thermal properties or low capacity in loading some fillers. Polypropylene (PP) and polypropylene based-blends are the main polymers used for packaging [19–21], textile industry and household appliances [22]. The advantage of PP is correlated to ease of processing, low cost, reasonable mechanical properties as well as good recyclability. However, one of the reasons that still suppresses the use of polypropylene as an engineering thermoplastic is the low impact strength, especially under conditions of low temperature and high deformation rates. One way to increase the use as an engineering polymer is the addition of elastomers [23, 24]. A common and the most useful strategy to overcome this limitation is to blend PP with an olefinic polymer, been largely applied in the industry [22]. The olefinic polymers applied to blend with PP to modify its impact strength are copolymers based on ethylene, like ethylene–vinyl acetate (EVA), which is also a low-cost polyolefin [22, 25, 26]. The contribution of EVA to improve the impact strength of PP has been proved [20, 25–27] such as the immiscibility between both polymers, due to their completely different chemical structures [25, 26, 28]. To overcome this problem, the addition of a compatibilizer agent may improve the interfacial adhesion

between the PP and EVA phases, modifying its morphology, hence increasing the mechanical properties of the PP/EVA blend [26, 29]. The main compatibilizer agent used in PP/EVA blends is the maleic anhydride grafted PP (PP-*g*-MA) [26, 29–31]. The advantage of PP-*g*-MA addition is the compatibilization efficiency of the blend, conferring greater and better adhesion between the phases (PP and EVA) and better distribution and dispersion of the EVA phase in the PP matrix [26, 29–31].

PP/EVA blends-based carbonaceous materials are an important method to improve the electrical conductivity of insulating materials [13]. Some studies about PP/EVA blends-based graphene [30] and carbon nanotubes [32–34] showed significant improvements in electrical conductivity. Liu et al. [33] prepared PP/EVA blends-based carbon nanotubes nanocomposites in a twin-screw extruder, and observed the formation of cocontinuous morphology and the filler was distributed preferably on the EVA phase.

In this work, a new PP/EVA blend-based carbonaceous material was developed using the glassy carbon (GC) as filler. The effect of the addition of maleic anhydride grafted PP (PP-*g*-MA) as compatibilizer agent and the addition of different contents of GC as filler to PP/EVA (60/40) blend in the thermal, mechanical, electrical and morphological properties were also investigated. The 60/40 blend ratio was adopted to obtain a cocontinuous morphology, according to Liu et al. [33]. This morphology was chosen for the reason that, if the GC particle lodges in the interfacial region, the percolation threshold tends to decrease, leading to the use of a smaller content of filler, decreasing the cost of production and decreasing the maleficent effects that fillers can cause in some properties of composites. Another goal is to expand the use of glassy carbon, a carbonaceous material that is easily obtainable and has excellent electrical properties.

2 Experimental

2.1 Materials

Polypropylene (PP) with specification H 301 with density of 0.905 g/cm³ and melt flow index (MFI) 10 g/10 min (2.16 kg, 230 °C).

Ethylene–vinyl acetate (EVA) with specification TN 2020 with 8.5 wt% of vinyl acetate (VA), the density of 0.931 g/cm³ and MFI 2.0 g/10 min (2.16 kg, 190 °C). The PP and EVA were supplied by Braskem (Brazil).

Maleic anhydride grafted polypropylene (PP-*g*-MA) with a trade name Polybond® 3200 (Crompton Corporation) with 1 wt% of maleic anhydride and MFI 10.1 g/10 min (2.16 kg, 230 °C).

The monolithic glassy carbon (GC) used was prepared on a laboratory scale.

2.2 Obtaining the glassy carbon (GC)

The monolithic glassy carbon (GC) was obtained by polymerizing furfuryl alcohol in the presence of an aqueous solution of a *p*-toluenesulfonic acid catalyst (APTS) (3% w/w) at a ratio of 60% w/v. The mixture was mechanically homogenized, centrifuged for 40 min at 3000 rpm, and poured into flat molds where it was kept at room temperature for 24 h. Subsequently, the mold was transferred to a kiln to continue the curing process maintaining the resin at 60 °C for 24 h, then at 80 °C for 2 h, at 110 °C for 2 h and at 180 °C for 6 h. The cured resin was then cut into specimens, and then heat-treated based on previous work [16], was executed in a tubular oven at a heating rate of 10 °C h⁻¹ under nitrogen flow (1.0 L h⁻¹), from room temperature to a maximum temperature of 1000 °C, which was held for 30 min. Subsequently, the oven was cooled naturally. After that, the resulting material was milled (IKA mini mill, model A11) at room temperature for use as a filler.

2.3 Characterization of the glassy carbon

The GC powder after the mill process was sieved in a 200 mesh metal sieve to obtain GC powder with particle size smaller than 45 μm. The particle size distribution curves were obtained using a CILAS particle analyzer (model 1190 L). The structural analysis of this carbonaceous material was verified by X-ray diffractometry (XRD) on a Rigaku Ultima IV diffractometer (PANalytical, X'pert Powder model), operating at 40 kV and 30 mA with Cu Kα radiation (λ = 1.54056 Å). The scanning speed used was 5° min⁻¹ over a 2θ range of 5° to 70°.

The interlayer spacing (i.e., the distance between the graphitic planes) (d_{002}) of the GC was calculated by Bragg's Law (Eq. 1):

$$d_{002} = \lambda / 2 \sin \theta \quad (1)$$

where θ represents the peak diffraction angle of the plane (002) and λ is the wavelength of the X-ray.

The verification of the GC stacking height (L_c) was performed using the Scherer equation (Eq. 2):

$$L_c = 0.9 \lambda / \beta \cos \theta \quad (2)$$

where θ is the Bragg angle related to (002) plane, λ is the wavelength of the X-rays and using the values of β obtained from the equation $\beta^2 = \beta_{\text{obs}}^2 - \beta_{\text{p}}^2$. The β_{obs} and β_{p} are the full widths at half maximum of the peak of diffraction of the sample and of a standard (usually the mica),

both obtained in the same operating conditions of the equipment.

The calculation of the GC stacking width (L_a) was performed using Eq. 3:

$$L_a = 1.84 \lambda / \beta \cos \theta \quad (3)$$

where θ is the Bragg angle related to (10) plane, λ is the wavelength of the X-rays and using the values of β obtained from the equation $\beta^2 = \beta_{\text{obs}}^2 - \beta_{\text{p}}^2$. The β_{obs} and β_{p} are the full width at half maximum of the peak of diffraction of the sample and of a standard (usually mica), both obtained in the same operating conditions of the equipment.)

2.4 Preparation of PP/EVA blends-based GC composites

The composites and blends were prepared in a molten state by the extrusion process following a similar methodology of previous works [16, 35]. Before the extrusion process, all materials were dried for 24 h in an oven at 80 °C. The neat materials (PP and EVA), PP/EVA blend (60/40) and PP/EVA/PP-*g*-MA (57/40/3) blend with the addition of 3 wt% of PP-*g*-MA were manually mixed and processed in a co-rotational twin-screw extruder, fabricated by AX Plásticos, model AX16:40DR, with $L/D = 40$ and $D = 16$ mm. The temperature profile applied was 170, 190, 190, 190 and 195 °C, and the screw speed set at 120 rpm.

The same conditions were used to prepare PP/EVA/PP-*g*-MA blends-based GC composites with the addition of 0.1, 0.5, 1, 3 and 5 wt% of GC. Table 1 shows the nomenclature used in this work. All the extrudates were pelletized at the die exit, dried, and then molded into test specimens using the hot compression process.

For all subsequent characterizations, test specimens for tensile tests and Izod impact strength were molded with 3.2 mm thick using a hydropneumatic press (MH Equipamentos, model PR8HP) at 200 °C for 3 min with a pressure of 2 bar. The test specimens molded were also used for thermal, electrical and morphological tests.

2.5 Characterization of PP/EVA blends-based GC composites

2.5.1 Thermal properties

Differential scanning calorimetry (DSC) and thermogravimetric analysis (TGA) were used to evaluate the thermal properties of the neat polymers, blend and composites.

Melting temperature (T_m) and crystallization temperature (T_c) were obtained by DSC using a NETZSCH, model 204 F1 Phoenix* equipment, using N₂ as the carrier gas.

Table 1 Nomenclature of the compositions studied

Nomenclature	Composition	PP (wt%)	EVA (wt%)	PP-g-MA (wt%)	Glassy carbon (wt%)
PP	PP	100	0	0	0
EVA	EVA	0	100	0	0
B	PP/EVA	60	40	0	0
CB	PP/EVA/PP-g-MA	57	40	3	0
GC 0.1%	PP/EVA/PP-g-MA/glassy carbon	56.94	39.96	3	0.1
GC 0.5%	PP/EVA/PP-g-MA/glassy carbon	56.7	39.8	3	0.5
GC 1%	PP/EVA/PP-g-MA/Glassy Carbon	56.4	39.6	3	1
GC 3%	PP/EVA/PP-g-MA/glassy carbon	55.2	38.8	3	3
GC 5%	PP/EVA/PP-g-MA/glassy carbon	54	38	3	5

DSC tests were performed with two heating cycles from 0 to 250 °C using a heat rate of 10 °C/min. The degree of crystallinity (X_c) of the compositions was determined according to Eq. 4

$$X_c = \left(\frac{\Delta H_m}{\Delta H_m^o} \right) \times \Phi_{\text{blend}} \times 100 \quad (4)$$

where X_c (%) is the degree of crystallinity, ΔH_m is the melting enthalpy obtained by DSC, ΔH_m^o is the theoretical melting heat value for 100% crystalline polymer (207 J/g for PP and PP-g-MA and 100 J/g for EVA [36] and Φ_{blend} is the mass fraction of the component in the blend. The ΔH_m^o value for the composites was calculated for each composition considering the mass fraction of the blend in the composite.

Thermogravimetric analysis (TGA) was performed using a NETZSCH Model TG 209 F1 Iris[®] equipment, under N₂ atmosphere, according to the following protocol: the samples were heated from room temperature to 800 °C at 20 °C/min. The degradation temperatures were analyzed for each composition tested.

2.5.2 Mechanical properties

Tensile tests were conducted on specimens using a MTS machine model Criterion 45 at a crosshead rate of 50 mm/min and load cell of 50 kN according to the ASTM D638-14. Five specimens were tested for each composition and the average value was calculated in each case.

The Izod impact strength tests were performed in a CEAST/Instron Impact Test Machine (model 9050) following the ASTM D256-06. The notches in the specimens were manually made in a notched machine (CEAST), and the impact load set was a hammer of 2.75 J. Seven specimens were tested for each composition and the average value was calculated in each case.

2.6 Fracture surface morphology

The fracture surface morphology was evaluated by scanning electron microscopy (SEM) using the impact test specimens. A scanning electron microscope (FEI Inspect S50) was operated at 15 kV to observe the fracture surfaces, which were supported by aluminum stubs and covered with a gold layer by sputtering.

2.7 Electrical characterization

The electrical characterization of the samples was performed by impedance spectroscopy and electrical resistivity AC (alternating current). The values of electrical conductivity (σ) were calculated from the inverse of the electrical resistivity (ρ) (Eq. 5), values that were obtained from the relation between the impedance values (Z) and the electrical contact area dimensions of the samples (A , area and l thickness), Eq. 6. A thin layer of gold/palladium alloy was deposited by a metallizer (MED020 Bal-tec) on both sides of the samples, to form the electrical contact, producing a metal–nanocomposite–metal structure.

$$\sigma = 1/\rho \quad (5)$$

$$\sigma = (Z \times A)/l \quad (6)$$

An impedance analyzer (Solartron SI 1260, Impedance/Gain-phase Analyzer), coupled to a computer interface, performed the impedance measurements at room temperature at a frequency of 1 Hz and a voltage amplitude of 0.5 V [16].

3 Results and discussion

3.1 Characterization of GC obtained

Figure 1a shows the particle size distribution results of the GC particles after the mill process. The average Fraunhofer diameter of particulate material is $22.50\ \mu\text{m}$ with a large particle size distribution. The values obtained are within the expected diameter range and it proves the efficiency of the milling method that was used.

The XRD diffractogram obtained for the GC are shown in Fig. 1b. It was possible to observe the presence of 2 characteristic peaks of a turbostratic structure. The peak located at 43.6° may be attributed to the plane (100) and is associated with in-plane structure. The peak at 23.6° , in turn, is attributed to the plane (002) and is related to the graphitic stacking structure [37, 38]. The d_{002} was calculated by Bragg's law (Eq. 1), resulting in $d_{002} = 0.377\ \text{nm}$. This interplanar distance is greater than the interplanar

distance in ideal graphite crystallites ($d_{002} = 0.335\ \text{nm}$) and indicates a larger amount of carbon plane stacking defects. Using the Scherer's equation (Eqs. 2 and 3), it was found that the values of crystallite stacking width (La) and stacking height (Lc) were $5.57\ \text{nm}$ and $1.00\ \text{nm}$, which are compatible with those presented in the literature [37]. Due to their disordered microstructure, the GC crystallites do not develop even under heat treatments at temperatures above $3000\ ^\circ\text{C}$ having larger interlayer spacing and smaller size (Lc and La) than the characteristic values for graphite [39, 40].

Figure 1c shows the SEM image for GC. It is possible to observe that the size of the GC particles ($< 45\ \mu\text{m}$) is according to the results obtained by the particle size distribution analysis. The morphology of the particulates shows a smooth surface and defined edges, which reveals the fragile characteristic of GC, with nonhomogeneous shapes and particle sizes similar to those observed by Santos et al. [16].

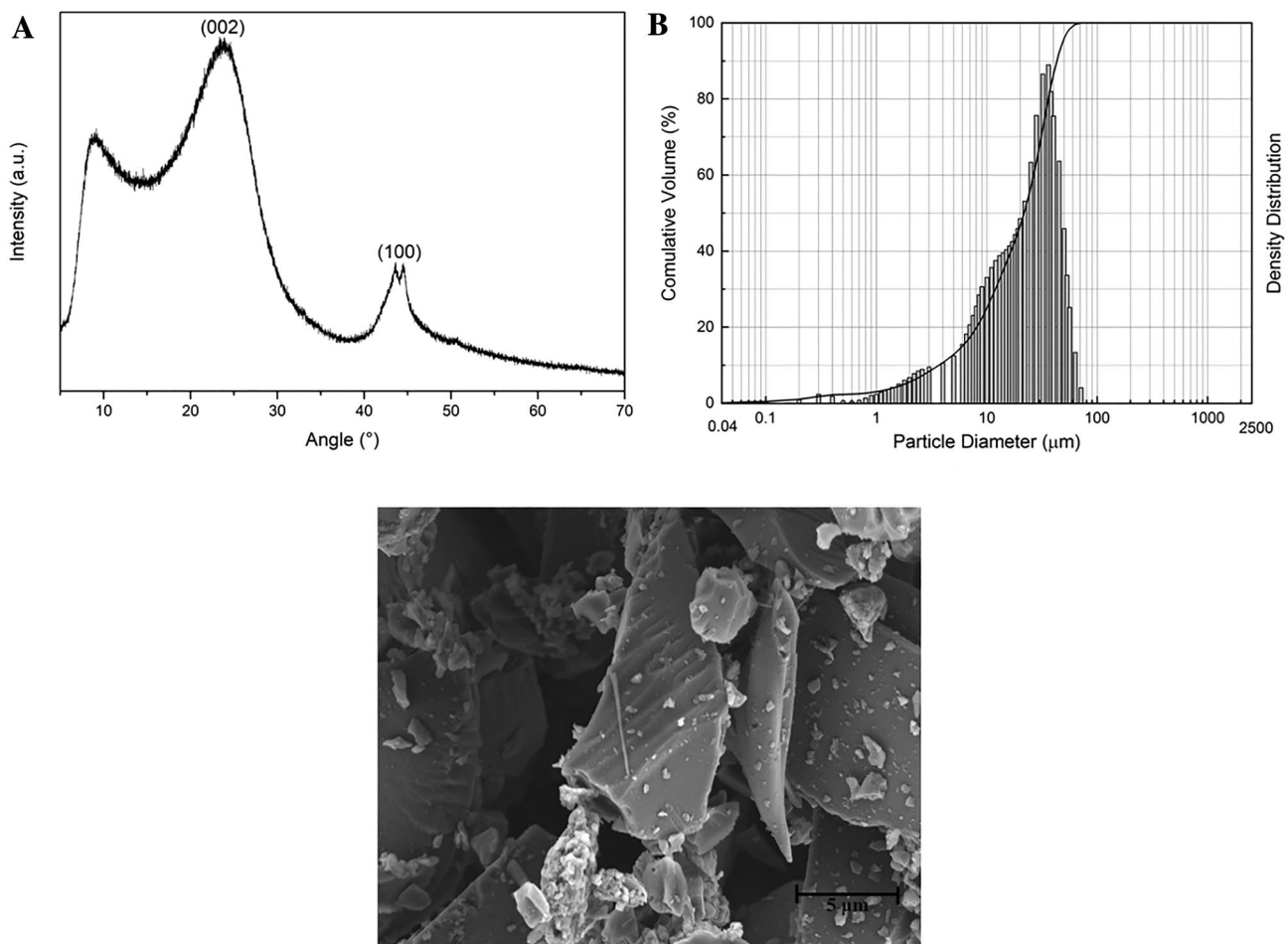


Fig. 1 The **a** X-ray diffractogram of GC, **b** particle size distribution and cumulative volume of the GC and **c** SEM image of GC's particles

3.2 Thermal analysis

Figure 2 shows the DSC curves and Table 2 shows the DSC results for all compositions. Both endothermic peaks observed in the blend (B), compatibilized blend (CB) and all the composites curves are associated to the melting temperature (T_m) of neat components, indicating an immiscibility between these polymers [41]. No changes in the T_m of EVA phase were observed for the blends and composites. On the other hand, a slight decrease on T_m of the PP phase was observed in PP/EVA blend and for all composites, probably associated to PP-g-MA addition as compatibilizer agent, which may facilitate the mobility of the polymeric chains during the fusion of the material. Crystallization temperature (T_c) values of EVA and PP had no significant change, indicating that PP and EVA did not influence on each other crystallization behavior [41, 42].

Regarding the crystallinity degree of PP and EVA phases in the blends and composites, PP and EVA phases in

composition B showed smaller crystallinity degrees than those presented in neat materials, which can be attributed to the presence of interfaces between phases that act as barrier for the mobility of polymer chains, resulting in more amorphous zones [43]. A new reduction in crystallinity degree of PP and EVA phases was observed in CB, with the addition PP-g-MA compatibilizer, which hinders the approximation of polymer chains and difficult the formation of organized structure. The addition of GC as filler results in an increase in the crystallinity degree for both polymers, which can be associated to the heterogeneous nucleation agent action of the GC, as other carbon materials such as carbon nanotubes act for thermoplastic polymers as PP [33].

The degradation behavior of neat materials (PP and EVA) and blends is presented in Table 3 and Fig. 3a and b. Firstly, by evaluating only the degradation temperatures for neat PP, a single degradation process is observed, in which the onset degradation temperature (T_{onset}) is approximately 421 °C. For neat EVA, two degradation stages are observed, one with a lower intensity that starts at a lower temperature around 354 °C, related to the vinyl groups present in the EVA chain, which for the material used was around 8.5% of the total weight as per manufacturer specification. The second degradation step may be associated to the polyethylene (PE) phase present in the

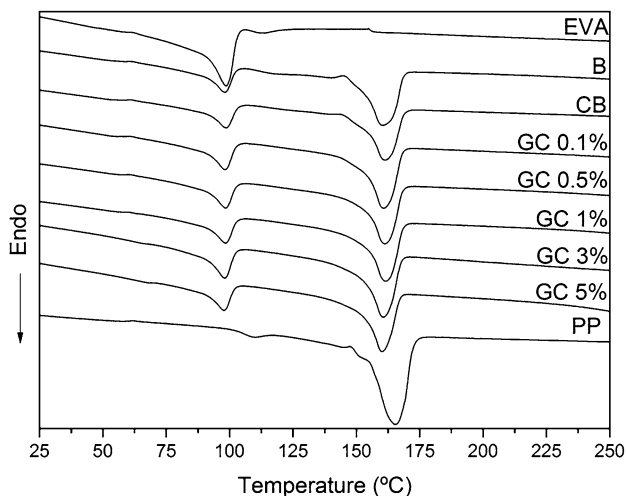


Fig. 2 DSC curves of the second heating scans of neat polymers (PP and EVA), blend (B), compatibilized bend (CB) and composites with different contents of GC

Table 3 TGA results for neat polymers (PP and EVA), blend (B), compatibilized bend (CB) and composites with different contents of GC

Composition	T_{onset} (°C)
PP	421
EVA	354/471
B	452
CB	449
GC 0.1%	444
GC 0.5%	454
GC 1%	462
GC 3%	437
GC 5%	454

Table 2 Values of T_c obtained during cooling scan, T_m , ΔH_m , and X_c obtained during second heating scans for neat polymers (PP and EVA), blend (B), compatibilized bend (CB) and composites with different contents of GC

Sample	Cooling		Second heat					
	$T_{c,PP}$ (°C)	$T_{c,EVA}$ (°C)	$T_{m,PP}$ (°C)	$\Delta H_{m,PP}$ (J/g)	$i_{c,PP}$ (%)	$T_{m,EVA}$ (°C)	$\Delta H_{m,EVA}$ (J/g)	$X_{c,EVA}$ (%)
PP	115	–	165	86	41	–	–	–
EVA	–	82	–	–	–	99	44	44
B	114	82	166	41	33	100	14	35
CB	116	82	161	36	29	99	13	33
GC 0.1%	116	82	161	44	36	98	15	38
GC 0.5%	116	82	161	45	36	98	13	33
GC 1%	117	82	162	43	35	98	12	31
GC 3%	117	83	161	44	36	98	17	44
GC 5%	117	83	160	47	40	98	14	37

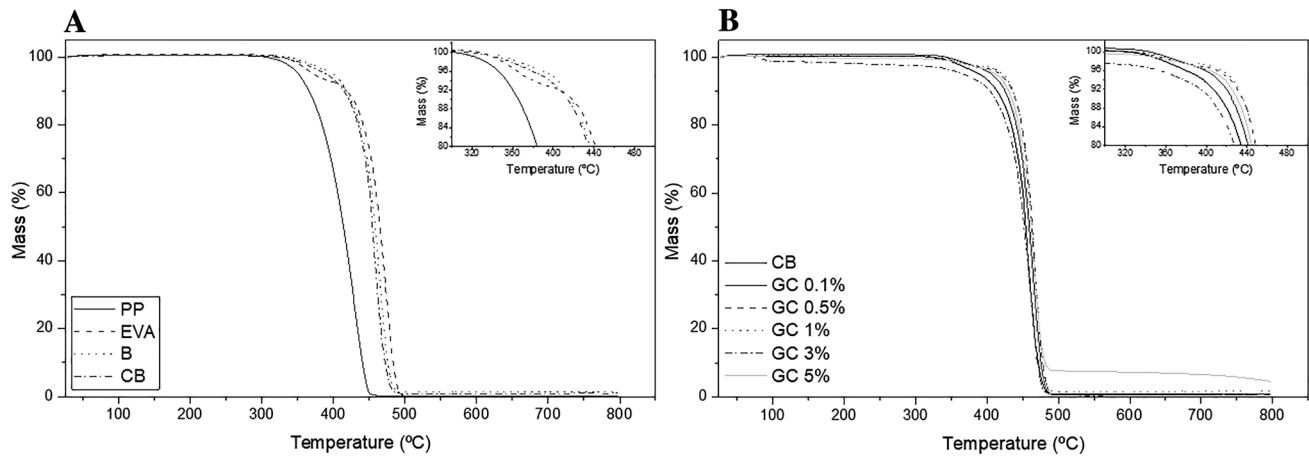


Fig. 3 TGA curves for **a** neat PP, neat EVA, blend (B) and compatibilized blend (CB) and **b** for the composites

EVA structure that occurred around 471 °C [41, 44, 45]. For the blends, the degradation curves appear as a single degradation step, where the initial degradation of EVA phase is attenuated and cannot be observed, since both phases (PP and EVA) begin their degradation at close temperatures. The composites showed an increase in T_{onset} values from 0.5% GC when compared to the compatibilized blend, with a maximum of 462 °C for the composition with the addition of 1% GC. This behavior is probably due to the higher thermal stability of the GC in comparison with the components of the blend, besides its good impermeability, which may generate a diffusion barrier to the gases arisen from the degradation of the material, increasing the thermal stability [37, 46, 47].

3.3 Morphological characterization

Figure 4a and b shows SEM micrographs of the non-compatibilized PP/EVA blend (B) and the compatibilized PP/EVA/PP-g-MA blend (CB) obtained after the Izod impact strength test. Analyzing the B micrograph (Fig. 4a), it is possible to observe the immiscibility of the components, where the EVA can be seen as a dispersed phase lodged throughout the PP phase. Due to the incompatibility of this system and the lack of a compatibilizer agent, the low interfacial adhesion between the phases resulted in a predominant fracture in the PP phase (indicated by the smooth regions) with low deformation of the EVA phase. In contrast, analyzing the CB morphology (Fig. 4b), it is possible to observe a higher interfacial adhesion, since the EVA phase deformed during the fracture, as shown by the circled region. However, it is still possible to observe smooth and voids due to EVA phase extractions, indicating a not very strong interface in certain regions of the CB provoked by a not sufficient mixture of the PP-g-MA in the blend. Goodarzi et al. [27] prepared PP/EVA blends with

the addition of 5 wt% of PP-g-MA. The authors verified for PP/EVA (75/25) blend a morphology of EVA droplets in PP matrix and for the 50/50 blend a completely cocontinuous morphology. For the blend 75/25, the use of 5 wt% of PP-g-MA increased the interfacial adhesion and decreased the size of the second phase and, for the 50/50 blend, resulted in a coarse co-continuous morphology. Therefore, for the PP/EVA (60/40) blend, a better interfacial adhesion can be expected for contents higher than 3 wt% of PP-g-MA.

Figure 4c and d shows SEM micrographs of the composites with addition of 0.5 and 1 wt% of GC. In the micrograph of the composite with the addition of 0.5 wt% of GC (Fig. 4c) it is possible to observe that the GC is preferentially lodged at the EVA phase, indicating that there is a low affinity for the PP. As the GC content increases to 1 wt% in the composite (Fig. 4d), it is possible to observe the formation of clusters, which is expected as the low affinity with the polymeric phases causes the smaller particles to migrate to the interface and agglomerate. As a result, there is a weakening of the interface, and consequently the composite toughness is reduced, which will be confirmed by the Izod impact strength test.

3.4 Mechanical properties

Table 4 shows the values of ultimate tensile strength (UTS), deformation at break (ϵ_b) and Young's modulus (E) for the compositions. PP presented the highest results when compared to the UTS among all the compositions, whereas EVA presented the lowest result. As expected for the immiscible blend system, the blends had intermediate properties between both polymers depending on their compositions, and better properties with an additive behavior were observed to CB in comparison with B [32, 35]. The incorporation of GC to the CB did not significantly change the material's UTS.

Fig. 4 SEM micrographs of **a** B composition (PP/EVA), **b** CB composition (PP/EVA/PP-g-MA), **c** composites with 0.5 wt% GC and **d** with 1 wt% GC

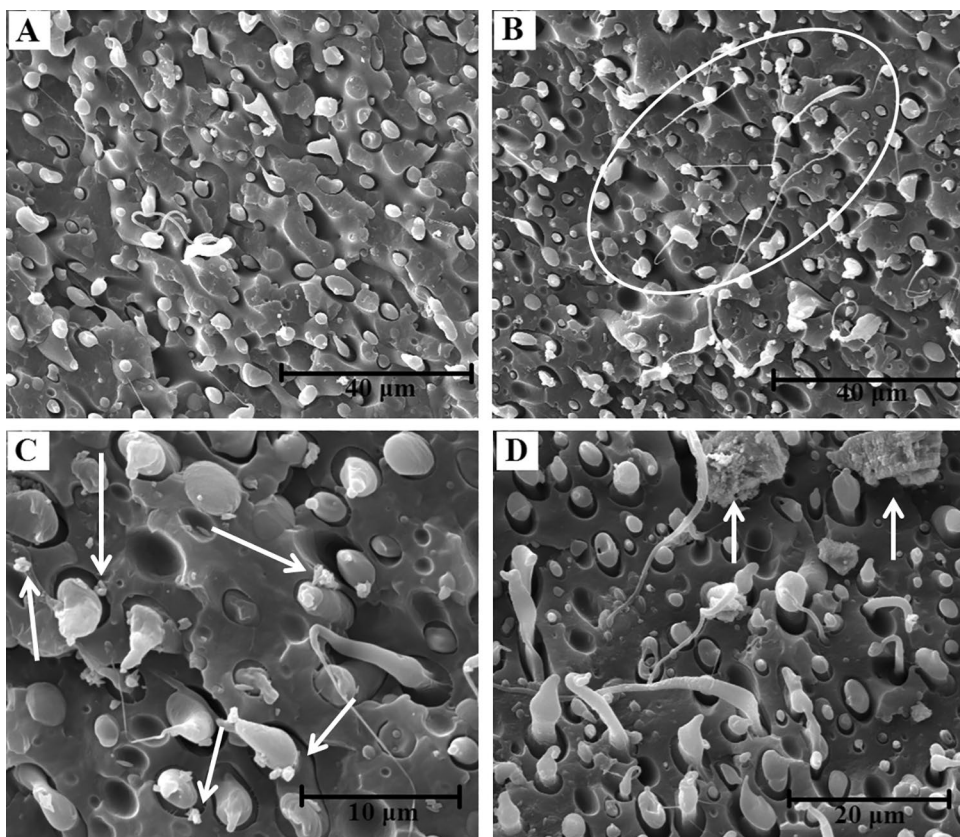


Table 4 Values of ultimate tensile strength (UTS), elongation at break (ϵ_r), Young’s modulus (E) and Impact strength for neat polymers (PP and EVA), blend (B), compatibilized bend (CB) and composites with different contents of GC

Compositions	Ultimate tensile strength (MPa)	Elongation at break (%)	Young’s modulus (MPa)	Impact strength (J/m)
PP	29.2 ± 0.7	10.2 ± 0.2	1004.6 ± 75.4	25 ^a
EVA	9.4 ± 0.1	Did not break	69.2 ± 5.6	Did not break
B	16.3 ± 0.4	19.4 ± 3.0	530.7 ± 5.9	33.8 ± 5.9
CB	17.6 ± 0.5	28.2 ± 3.8	624.7 ± 11.4	39.4 ± 3.0
GC 0.1%	18.5 ± 0.4	18.0 ± 3.5	668.5 ± 8.6	39.8 ± 2.3
GC 0.5%	17.7 ± 0.6	14.4 ± 2.7	607.3 ± 9.6	39.7 ± 3.4
GC 1%	17.1 ± 0.2	17.5 ± 3.1	581.3 ± 4.8	40.7 ± 4.3
GC 3%	17.1 ± 0.8	12.5 ± 1.3	592.7 ± 22.0	34.8 ± 1.4
GC 5%	18.2 ± 0.5	9.6 ± 1.0	682.0 ± 12.3	32.2 ± 1.4

^aMaterial data sheet information

The addition of a high tenacity material (EVA) significantly increased the deformation at break value of neat PP (10.2 ± 0.2%), as can be seen in B (19.4 ± 3%). The use of the compatibilizer agent improved the adhesion between the EVA and PP phases in the blends, since CB presented greater deformation at break (28.2 ± 3.8%) than B. It can also be seen from Table 4 that the addition of different GC contents to the compatible blend reduced the deformation at break of this material, which can be explained by

the restriction of the relative displacement between the polymer chains caused by the friction with GC particles, as it was also observed by Silva et al. [9] with the addition of high contents of carbon black in PA6/LLDPE blends.

The addition of a rigid filler to a polymer matrix increases its elastic modulus [9]. As observed in Table 4, this behavior was proven in GC 0.1% and GC 5% composites. For GC 0.5% and GC 3%, however, there was no significant change. The addition of 1 wt% GC in the blend,

in turn, decreased this property, which can be explained by a possible agglomeration of particulate material in the polymer matrix, impairing the formation of the interface. The ultimate tensile strength increases for the composites with the addition of 0.1 and 5 wt% GC, which might be associated with the increase in the crystallinity degree of PP and EVA phase for these compositions [9].

Table 4 also presents the Izod impact strength results. The EVA specimens did not break during the impact test, confirming its good impact strength. PP and EVA are immiscible phases and may present a weak interface, which causes a decrease in mechanical properties of the blends and composites when compared to the neat EVA [31, 34]. It is also verified that the addition of EVA provided a toughening to the PP matrix, since the blends and composites presented higher impact strength values than the neat PP. The addition of PP-*g*-MA improved the impact strength of CB compared to B, indicating an improvement in the interface between the existing PP and EVA phases. The incorporation of 0.1 to 1 wt% of GC to CB had preserved the impact strength in the composites, but higher contents of GC (3 and 5 wt%) resulted in a decrease in the impact strength as expected with a stiff filler as observed for the higher content of carbon black in PA6/LLDPE blends [9].

3.5 Electrical characterization of composites

The results of the electrical impedance spectroscopy of the neat polymers, blends and composites are shown in Table 5. Figure 5 shows the electrical conductivity of the compatibilized blend and the composites. It is possible to verify that the addition of different contents of GC to the compatibilized blend resulted in just a slight decrease in the electrical resistivity. It was observed that CB presented an electrical resistivity of $2.88 \times 10^{+13} \Omega \text{ m}$

Table 5 Values of electrical conductivity and electrical resistivity for neat polymers (PP and EVA), blend (B), compatibilized bend (CB) and composites with different contents of GC

Compositions	Electrical conductivity (S/m)	Electrical resistivity ($\Omega \text{ m}$)
PP	7.28×10^{-14}	$1.37 \times 10^{+13}$
EVA	1.71×10^{-14}	$5.84 \times 10^{+13}$
B	5.29×10^{-14}	$1.89 \times 10^{+13}$
CB	3.47×10^{-14}	$2.88 \times 10^{+13}$
GC 0.1%	2.44×10^{-13}	$4.10 \times 10^{+12}$
GC 0.5%	5.09×10^{-13}	$1.97 \times 10^{+12}$
GC 1%	3.18×10^{-13}	$3.14 \times 10^{+12}$
GC 3%	2.99×10^{-13}	$3.35 \times 10^{+12}$
GC 5%	6.23×10^{-13}	$1.61 \times 10^{+12}$

and an electrical conductivity of $3.47 \times 10^{-14} \text{ S/m}$, whereas the composite with the highest GC content (5 wt%) presented an electrical conductivity of one order of magnitude greater, $6.23 \times 10^{-13} \text{ S/m}$. The explanation for this fact can be given from the analysis of the micrographs, as can be seen from Fig. 4c and d. The morphology of the blend obtained presents a disperse phase of EVA throughout the PP matrix, with the GC particles lodged preferably in the EVA phase. In this way, GC particles formed clusters that do not establish physical contact with each other, and the low distribution and dispersion of the GC negatively affected the formation of an electron conduction path through the polymeric blend, impairing the electrical percolation. A similar behavior was observed by Han et al. [48] using multi-wall carbon nanotubes (MWCNT) in another immiscible blend as matrix.

GC can be used as conductive filler and contributes to increase the electrical conductivity of composites [16]. However, there must be connection points between GC particles to form a percolative path. In this case, as the GC is preferably in one phase (EVA), there is a lower probability of contacts between the GC particles, which promoted a slight modification in the electrical conductivity. Figure 6 presents a schematic of the morphology presented for the composites. It is possible to observe that the GC can be found either in the EVA phase or in the interface between the phases. For a significant increase in electrical conductivity to occur, a surface modification of the GC must be made so that it is distributed throughout the matrix, increasing the contact between the GC particles.

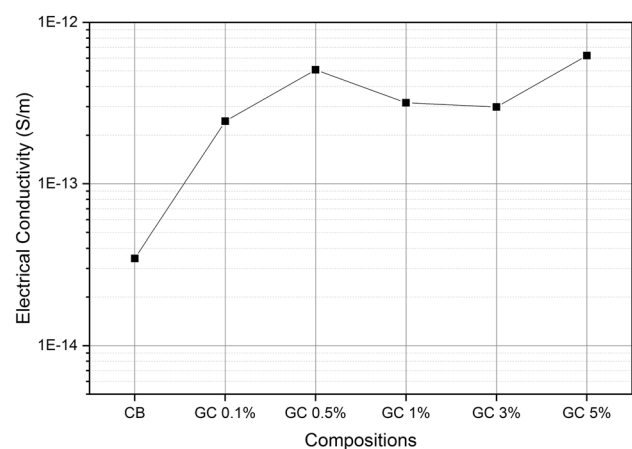
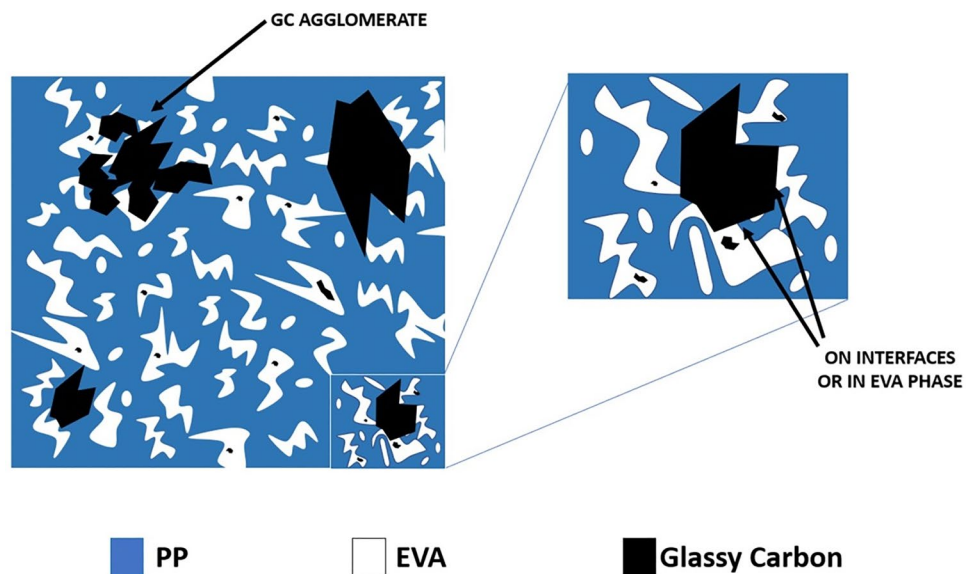


Fig. 5 Electrical conductivity for the compatibilized blends (CB) and for the composites as a function of GC content

Fig. 6 PP/EVA blends-based GC composites morphology scheme showing the preferred location of the GC in the EVA phase and at the interface between EVA and PP at GC content greater than 0.5 wt%



4 Conclusions

PP/EVA blends-based GC composites were processed and characterized by thermal, mechanical, morphological and electrical analyses. The DSC results show that the blends and composites are immiscible and a heterogeneous nucleation effect of GC to EVA on the blends increasing the crystallinity degree. The GC addition between 0.5 and 1 wt% improves the thermal stability of the PP/EVA blend. A disperse morphology was observed for PP/EVA blend, which also has a higher interfacial adhesion for a compatibilized blend. The morphologies of the composites indicate a preferential location of the GC on interfacial regions and EVA phase. Mechanical properties were improved with the addition of PP-*g*-MA as a compatibilizer agent, and the addition of GC in 0.1 wt% promotes an increase in the elastic modulus and UTS with no significant loss in the impact strength comparing to the compatibilized PP/EVA blend. However, increases in the GC content in the PP/EVA blend had no significant influence on the mechanical properties. From electrical analysis, the addition of GC showed a slight increase in electrical conductivity.

Acknowledgements This study was designed as a final project for post graduate students of the Post Graduate Program in Engineering and Materials Science (PPG-ECM) at Federal University of São Paulo (UNIFESP) of São José dos Campos (Brazil). This study was financed in part by the Coordenação de Aperfeiçoamento Pessoal de Nível Superior – Brasil (CAPES) – Finance Code. The authors are grateful to FAPESP (Process 2018/09531-2) for the financial support. The authors also thank Dr. Larissa Stieven Montagna for all contributions and analysis.

Compliance with ethical standards

Conflict of interest The authors declare that they have no conflict of interest.

References

- Jenkins GM, Kawamura K (1971) Structure of glassy carbon. *Nature*. <https://doi.org/10.1038/231175a0>
- Craievich AF (1976) On the structure of glassy carbon. *Mater Res Bull*. [https://doi.org/10.1016/0025-5408\(76\)90029-5](https://doi.org/10.1016/0025-5408(76)90029-5)
- Sakintuna B, Yürüm Y (2005) Templated porous carbons: a review article. *Ind Eng Chem Res* 44:2893–2902
- Sharma S (2018) Glassy carbon: a promising material for microand nanomanufacturing. *Materials (Basel)* 11:1857
- Noda T, Inagaki M, Yamada S (1969) Glass-like carbons. *J Non Cryst Solids*. [https://doi.org/10.1016/0022-3093\(69\)90026-X](https://doi.org/10.1016/0022-3093(69)90026-X)
- Hokao M, Hironaka S, Suda Y, Yamamoto Y (2000) Friction and wear properties of graphite/glassy carbon composites. *Wear*. [https://doi.org/10.1016/S0043-1648\(99\)00306-3](https://doi.org/10.1016/S0043-1648(99)00306-3)
- Botelho EC, Scherbakoff N, Rezende MC (2001) Porosity control in glassy carbon by rheological study of the furfuryl resin. *Carbon N.Y.* [https://doi.org/10.1016/S0008-6223\(00\)00080-4](https://doi.org/10.1016/S0008-6223(00)00080-4)
- Huang J-C (2002) Carbon black filled conducting polymers and polymer blends. *Adv Polym Technol* 21:299–313. <https://doi.org/10.1002/adv.10025>
- Silva LN, Anjos EGR, Morgado GFM (2019) Development of antistatic packaging of polyamide 6/linear low—density polyethylene blends—based carbon black composites. *Polym Bull*. <https://doi.org/10.1007/s00289-019-02928-3>
- da Silva TF, Menezes F, Montagna LS et al (2019) Preparation and characterization of antistatic packaging for electronic components based on poly(lactic acid)/carbon black composites. *J Appl Polym Sci* 136:47273. <https://doi.org/10.1002/app.47273>

11. Cardinaud R, McNally T (2013) Localization of MWCNTs in PET/LDPE blends. *Eur Polym J* 49:1287–1297. <https://doi.org/10.1016/j.eurpolymj.2013.01.007>
12. Vadukumpully S, Paul J, Mahanta N, Valiyaveetil S (2011) Flexible conductive graphene/poly(vinyl chloride) composite thin films with high mechanical strength and thermal stability. *Carbon N Y* 49:198–205. <https://doi.org/10.1016/j.carbon.2010.09.004>
13. Rahaman M (2019) Carbon-containing polymer composites. Springer, Singapore
14. Tian Y, Zhang X, Geng H-Z et al (2017) Carbon nanotube/polyurethane films with high transparency, low sheet resistance and strong adhesion for antistatic application. *RSC Adv* 7:53018–53024. <https://doi.org/10.1039/C7RA10092B>
15. Szeluga U, Pusz S, Kumanek B et al (2016) Influence of unique structure of glassy carbon on morphology and properties of its epoxy-based binary composites and hybrid composites with carbon nanotubes. *Compos Sci Technol* 134:72–80. <https://doi.org/10.1016/j.compscitech.2016.08.004>
16. dos Santos MS, Montagna LS, Rezende MC, Passador FR (2019) A new use for glassy carbon: development of LDPE/glassy carbon composites for antistatic packaging applications. *J Appl Polym Sci* 136:1–8. <https://doi.org/10.1002/app.47204>
17. Bressmann T (2003) Polymer blends handbook. Springer, Berlin
18. Paul DR (1978) Polymer blends vol 1. *J Chem Inf Model* 53:1689–1699. <https://doi.org/10.1017/CBO9781107415324.004>
19. Aghjeh MR, Khonakdar HA, Jafari SH (2015) Application of mean-field theory in PP/EVA blends by focusing on dynamic mechanical properties in correlation with miscibility analysis. *Compos Part B Eng* 79:74–82. <https://doi.org/10.1016/j.compositesb.2015.04.026>
20. Zhang Y, Li J, Shen L et al (2017) The observation of PP/EVA blends in which isotactic PP was preradiated with different radiation absorbed doses. *J Appl Polym Sci* 134:1–7. <https://doi.org/10.1002/app.45057>
21. Nikoomeanesh R, Naderpour N, Goodarzi V et al (2019) Prediction of mechanical properties of PP/EVA polymer blends governed by EVA phase change in the presence of environmentally friendly inorganic tungsten disulfide nanotubes (INT-WS 2). *Polym Compos* 40:1964–1978. <https://doi.org/10.1002/pc.24972>
22. Albizzati E, Giannini U, Collina G et al (2019) Polypropylene handbook. Springer, Cham
23. Gupta AK, Ratnam BK, Srinivasan KR (1992) Melt-rheological properties of PP/EVA blend. *J Appl Polym Sci* 46:281–293. <https://doi.org/10.1002/app.1992.070460209>
24. Öksüz M, Eroğlu M (2005) Effect of the elastomer type on the microstructure and mechanical properties of polypropylene. *J Appl Polym Sci*. <https://doi.org/10.1002/app.22271>
25. Ying X, Qinglong R, Fengfeng Z et al (2016) Study on the toughening mechanism of PP/EVA dynamically crosslinked blend. *J Macromol Sci Part A Pure Appl Chem* 53:523–529. <https://doi.org/10.1080/10601325.2016.1189286>
26. Maciel A, Salas V, Manero O (2005) PP/EVA blends: mechanical properties and morphology. effect of compatibilizers on the impact behavior. *Adv Polym Technol* 24:241–252. <https://doi.org/10.1002/adv.20050>
27. Goodarzi V, Jafari SH, Khonakdar HA et al (2012) Correlation of morphological, dynamic mechanical, and thermal properties in compatibilized polypropylene/ethylene-vinyl acetate copolymer/organoclay nanocomposites. *J Appl Polym Sci* 125:922–934. <https://doi.org/10.1002/app.33849>
28. Canto LB (2014) On the coarsening of the phase morphology of PP/EVA blends during compounding in a twin screw extruder. *Polym Test* 34:175–182. <https://doi.org/10.1016/j.polymertesting.2014.01.012>
29. Martins CG, Larocca NM, Paul DR, Pessan LA (2009) Nanocomposites formed from polypropylene/EVA blends. *Polymer (Guildf)* 50:1743–1754. <https://doi.org/10.1016/j.polymer.2009.01.059>
30. Varghese AM, Rangaraj VM, Mun SC et al (2018) Effect of graphene on polypropylene/maleic anhydride-graft-ethylene-vinyl acetate (PP/EVA-g-MA) blend: mechanical, thermal, morphological, and rheological properties. *Ind Eng Chem Res* 57:7834–7845. <https://doi.org/10.1021/acs.iecr.7b04932>
31. Ramírez-Vargas E, Navarro-Rodríguez D, Huerta-Martínez BM et al (2000) Morphological and mechanical properties of polypropylene [PP]/poly(ethylene vinyl acetate) [EVA] blends. I. Homopolymer PP/EVA systems. *Polym Eng Sci* 40:2241–2250. <https://doi.org/10.1002/pen.11356>
32. Liu L, Wang Y, Li Y et al (2009) Studies on fracture behaviors of immiscible polypropylene/ethylene-co-vinyl acetate blends with multiwalled carbon nanotubes. *J Polym Sci, Part B: Polym Phys* 47:1331–1344. <https://doi.org/10.1002/polb.21738>
33. Liu L, Wu H, Wang Y et al (2010) Selective distribution, reinforcement, and toughening roles of MWCNTs in immiscible polypropylene/ethylene-co-vinyl acetate blends. *J Polym Sci, Part B: Polym Phys* 48:1882–1892. <https://doi.org/10.1002/polb.22063>
34. Liu L, Wang Y, Li Y et al (2009) Improved fracture toughness of immiscible polypropylene/ethylene-co-vinyl acetate blends with multiwalled carbon nanotubes. *Polymer (Guildf)* 50:3072–3078. <https://doi.org/10.1016/j.polymer.2009.04.067>
35. dos Anjos EGR, Backes EH, Marini J et al (2019) Effect of LLDPE-g-MA on the rheological, thermal, mechanical properties and morphological characteristic of PA6/LLDPE blends. *J Polym Res* 26:1–10. <https://doi.org/10.1007/s10965-019-1800-y>
36. Wunderlich B (2013) Macromolecular physics. Elsevier, Amsterdam
37. Oishi SS, Botelho EC, Rezende MC, Ferreira NG (2017) Structural and surface functionality changes in reticulated vitreous carbon produced from poly(furfuryl alcohol) with sodium hydroxide additions. *Appl Surf Sci* 394:87–97. <https://doi.org/10.1016/j.apsusc.2016.10.112>
38. Kalijadis A, Jovanović Z, Laušević M, Laušević Z (2011) The effect of boron incorporation on the structure and properties of glassy carbon. *Carbon N Y*. <https://doi.org/10.1016/j.carbon.2011.02.054>
39. Inagaki M, Kang F (2014) Materials science and engineering of carbon: fundamentals. Butterworth-Heinemann, Oxford
40. Cheng L-T, Tseng WJ (2010) Effect of acid treatment on structure and morphology of carbons prepared from pyrolysis of polyfurfuryl alcohol. *J Polym Res* 17:391–399. <https://doi.org/10.1007/s10965-009-9325-4>
41. Palacios J, Perera R, Rosales C et al (2012) Thermal degradation kinetics of PP/OMMT nanocomposites with mPE and EVA. *Polym Degrad Stab* 97:729–737. <https://doi.org/10.1016/j.polymdegradstab.2012.02.009>
42. Zhang F, Li Q, Liu Y et al (2016) Improved thermal conductivity of polycarbonate composites filled with hybrid exfoliated graphite/multi-walled carbon nanotube fillers. *J Therm Anal Calorim* 123:431–437. <https://doi.org/10.1007/s10973-015-4903-7>
43. Kakkar D, Maiti SN (2012) Effect of flexibility of ethylene vinyl acetate and crystallization of polypropylene on the mechanical properties of i-PP/EVA blends. *J Appl Polym Sci* 123:1905–1912. <https://doi.org/10.1002/app.34680>
44. Jansen P, Soares BG (1996) Effect of compatibilizer and curing system on the thermal degradation of natural rubber/EVA copolymer blends. *Polym Degrad Stab* 52:95–99. [https://doi.org/10.1016/0141-3910\(95\)00238-3](https://doi.org/10.1016/0141-3910(95)00238-3)
45. Dikobe DG, Luyt AS (2010) Morphology and thermal properties of maleic anhydride grafted polypropylene/ethylene-vinyl

- acetate copolymer/wood powder blend composites. *J Appl Polym Sci* 11:6. <https://doi.org/10.1002/app.31630>
46. Jacobsen AJ, Mahoney S, Carter WB, Nutt S (2011) Vitreous carbon micro-lattice structures. *Carbon N Y*. <https://doi.org/10.1016/j.carbon.2010.10.059>
47. Chatterjee A, Deopura BL (2006) Thermal stability of polypropylene/carbon nanofiber composite. *J Appl Polym Sci*. <https://doi.org/10.1002/app.22864>
48. Han IS, Lee YK, Lee HS et al (2014) Effects of multi-walled carbon nanotube (MWCNT) dispersion and compatibilizer on the electrical and rheological properties of polycarbonate/poly(acrylonitrile-butadiene-styrene)/MWCNT composites. *J Mater Sci* 49:4522–4529. <https://doi.org/10.1007/s10853-014-8152-0>

Publisher's Note Springer Nature remains neutral with regard to jurisdictional claims in published maps and institutional affiliations.